12th International Symposium on Turbulence and Shear Flow Phenomena (TSFP12)
Osaka, Japan (Online), July 19-22, 2022

MODULATION OF HOMOGENEOUS ISOTROPIC TURBULENCE BY DISPERSED FIBRES AND PARTICLES

Ianto Cannon
Complex fluids and flows
Okinawa Institute of Science & Technology
1919-1 Tancha, Onna-son, Okinawa, 904-0495, Japan
ianto.cannon@oist.jp

Stefano Olivieri and **Marco E. Rosti**
Complex fluids and flows
Okinawa Institute of Science & Technology
1919-1 Tancha, Onna-son, Okinawa, 904-0495, Japan
stefano.olivieri@oist.jp and marco.rosti@oist.jp

ABSTRACT

We compare how a homogeneous isotropic turbulent flow (micro-scale Reynolds number $Re_\lambda \approx 435$) is modulated by finite diameter spheres and finite length fibres. Both spheres and fibres produce a similar bulk effect, characterized by a reduction of the micro-scale Reynolds number to around $Re_\lambda \approx 220$. However, a spectral analysis of the flows reveals very different stories for the two particle geometries. For spheres, the flow is modulated on scales comparable with the sphere diameter. Little modulation occurs at smaller scales, and the canonical turbulent energy cascade is recovered in this region of the spectra. While for fibres, modulation occurs over a much wider range of length-scales, (including the fibre thickness) and a new turbulent kinetic energy scaling $E \sim \kappa^{-1}$ is found in the place of the canonical cascade.

INTRODUCTION

Particles of many different shapes are found in turbulent flows, ranging from spherical pollen particles in the atmosphere to elongated plastic microfibres in the ocean (Kane & Clare, 2019) and cellulose fibres involved in papermaking (Lundell *et al.*, 2011). Understanding how these different particle shapes affect the flow is of environmental and industrial importance (De Lillo *et al.*, 2014; Breard *et al.*, 2016; Sengupta *et al.*, 2017; Falkinhoff *et al.*, 2020; Rosti *et al.*, 2020*b*). Here we investigate how the shape of the dispersed particles affects the flow. We explore two extremes of particle shape; perfectly isotropic spheres and highly anisotropic elongated fibres. Throughout this article, we will use "particle" as a general term to refer to both spheres and fibres.

Elghobashi (1994) gives a good overview of the dimensionless parameters that can be used to describe particle laden turbulent flows, including Stokes number, Galileo number, and particle volume fraction. In this work we focus on the effect of particle mass fraction $M \equiv m_p/(m_p+m_f)$, where m_p is the total mass of the particles, and m_f is the total mass of the fluid.

The majority of previous numerical investigations of particle laden turbulent flows consider only dilute suspensions ($M << 1$), where it is assumed the flow is not altered by presence of the particles (Balachandar & Eaton, 2010; Maxey, 2017; Brandt & Coletti, 2021). A few studies consider non-dilute suspensions of droplets (Dodd & Ferrante, 2016; Freund & Ferrante, 2019; Rosti *et al.*, 2019; Cannon *et al.*, 2021), isotropic particles (Lucci *et al.*, 2010; Gualtieri *et al.*, 2013; Capecelatro *et al.*, 2018; Ardekani *et al.*, 2019; Sozza *et al.*, 2020), and anisotropic particles (Andersson *et al.*, 2012; Olivieri *et al.*, 2020*a*,*b*, 2021). In these studies, authors report changes in the bulk flow properties, as well changes in the turbulent kinetic energy spectrum. In this work, we build on these studies by investigating non-dilute suspensions of finite sized particles[1]. In particular we directly compare homogeneous isotropic flows laden with spheres and fibres in order to ask the question, "how does the shape of the particles affect the flow?"

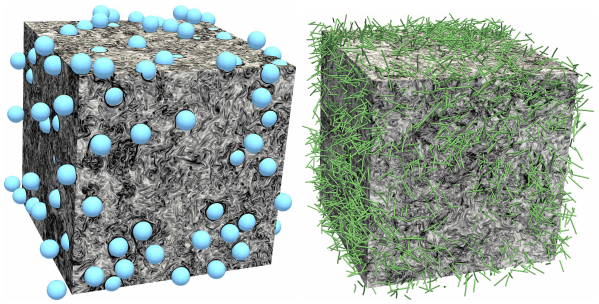

Figure 1. 3-D views of the fluid vorticity magnitude in the tri-periodic cubic domain with spheres (left), and fibres (right).

Figure 1 shows two snapshots of setups with spheres and fibres that we use to answer the above question. We performed direct numerical simulations of an incompressible Newtonian fluid in a tri-periodic cubic box of size L, discretised to 1024 numerical grid points in each of the three Cartesian directions. The fluid is coupled to particle dynamics using the immersed boundary method. See Podvigina & Pouquet (1994); Pope

[1] finite sized particles have a size which is comparable to the inertial range of the flow

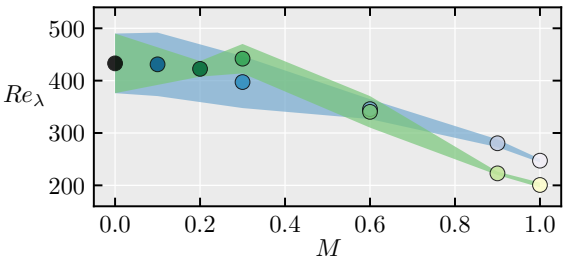

Figure 2. The micro-scale Reynolds number Re_λ as a function of the particle mass fraction M. Flows with spheres are marked in blue and flows with fibres are marked in green. The shaded blue and green regions show the standard deviation in Re_λ from the time averaged value.

(2000); Olivieri *et al.* (2021); Kim & Peskin (2007); Hori *et al.* (2022); Huang *et al.* (2007); Olivieri *et al.* (2020*a*,*b*); Rosti *et al.* (2020*a*); Rosti & Brandt (2020); Rosti *et al.* (2020*b*, 2021) for details and validation of the numerical method.

The flow is sustained by deterministic Arnold-Beltrami-Childress forcing (Podvigina & Pouquet, 1994), giving a micro-scale Reynolds number $Re_\lambda = u'\lambda/\nu \approx 435$ in the single phase flow, where ν is the kinematic viscosity, λ is Taylor's micro-scale, and u' is the root mean square of the turbulent fluctuations in fluid velocity. For the particles, we use 300 rigid spheres of diameter $c = L/(4\pi)$, or 10^4 fibres of identical length $c = L/(4\pi)$. These parameter choices give particles which have a similar total surface area, as well as being the same proportions. The numerical method is such that the fibres are slightly flexible, but their stiffness was set to a large value so their deformation was always negligible. The diameter of the fibres is $d \approx 2\Delta x = L/512$, determined by the smoothing of the Dirac delta function used in the immersed boundary method. We vary the density of the particles to give a range of mass fractions M. Note that $M = 0$ refers to the single phase case, and $M = 1$ refers to cases with particles fixed at random locations in the domain. The plots discussed in the following section were produced from time averaged simulations once they had been allowed to reach a statistically steady state.

RESULTS AND DISCUSSION

Figure 2 shows the effect of increasing particle mass fraction M on the micro-scale Reynolds number Re_λ of the flow. We see that Re_λ decreases in a similar fashion for increasing inertia of spheres and fibres alike. In addition, the standard deviation of Re_λ decreases with M, this is typical of a transition towards laminar flow, where oscillations in time are suppressed. Overall, from figure 2 we see that the isotropic and anisotropic particles have a similar effect on the bulk flow. To see the difference between the back-reactions of spheres and fibres we must observe the flows at all length scales.

Figure 3 shows the turbulent kinetic energy spectrum of each flow, with the Kolmogorov scaling $E \sim \kappa^{-5/3}$ for comparison. As expected, the single phase flow follows the canonical Kolmogorov scaling in the inertial range and is dominated by dissipation at the small scales ($\kappa > 100$). At the largest scales ($\kappa < 3$) we see the spheres and fibres produce a similar reduction in turbulent kinetic energy E relative to the single phase, that is, E reduces as the mass fraction M increases. At the smallest scales ($\kappa > 100$), we see that both spheres

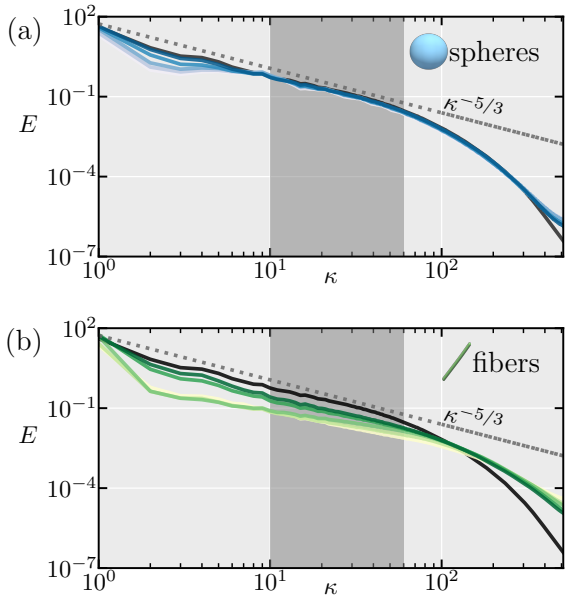

Figure 3. Energy spectra of the turbulent flows laden with (a) spheres and (b) fibres. The particle mass fraction M for each case is denoted by the brightness of the line colour, using the same colours as the markers in figures 2 and 4. The single phase flow is marked by a black line on both (a) and (b). The canonical Kolmogorov scaling is marked by a grey dotted line. The region in which we observe power law scalings ($10 < \kappa < 60$) is shaded in dark grey.

and fibres cause a turbulent kinetic energy increase relative to the single phase, and the effect is most pronounced in the case of fibres. As we shall see later, this is due to the fluid solid coupling which injects energy to the flow at small scales. The most pronounced difference between spheres and fibres is found at intermediate wave-numbers ($10 < \kappa < 60$). With spheres, the flow recovers to the single phase value of turbulent kinetic energy. Whereas with fibres, the energy is reduced and the canonical inertial scaling is not observed. Clearly the isotropic and anisotropic particles are interacting differently with the flow in this intermediate wave-number range. In all of the cases, we see clear power-law scalings (straight lines on the log-log scale), so we made power law fits $E = A\kappa^{-\beta}$ to the turbulent kinetic energy in the range $10 < \kappa < 60$, where A and β are fitted parameters.

Figure 4 shows the dependence of the fitted exponent β on the mass fraction M of particles. The single phase flow ($M = 0$) and the flows with spheres can be seen to follow the Kolmogorov scaling ($\beta = 5/3$), whereas the flows with fibres show a significant departure from Kolmogorov's theory as the mass fraction increases; and we see instead that $\beta \approx 1$ for $M > 0.6$. We explain the mechanism underlying this new scaling by considering the two point velocity correlations $\delta u(r)$ in the flows; $\delta u(r)$ is defined as the difference in fluid velocities at two points separated by a distance r. By simple dimensional analysis we expect the energy spectrum to scale linearly with the variance of the velocity correlation $\langle(\delta u(r))^2$;

$$E(\kappa) \sim \langle(\delta u(r))^2\rangle \kappa^{-1} \tag{1}$$

The fibres are slender, and they act as a barrier to the flow between any two points with separation greater than the fibre

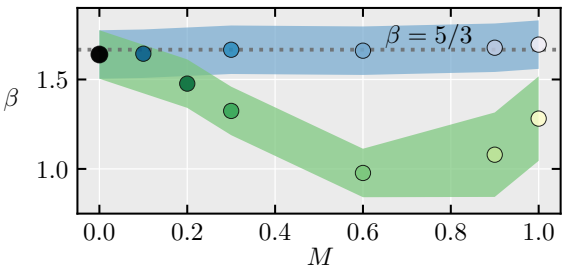

Figure 4. Dependence of the exponent β in the turbulent kinetic energy scaling $E \sim \kappa^{-\beta}$ on particle mass fraction M. Flows with spheres are marked in blue, flows with fibres in green, and the single phase flow in black. The blue and green shaded regions show the approximate error in β, estimated by moving the time averaging window. The Kolmogorov scaling is marked by a grey dotted line.

diameter d. Hence fibres decorrelate the flow by increasing the value of $\delta u(r)$ for all $r > d$. This means the variance of the correlation has little dependence on the separation, and so $\langle(\delta u(r))^2\rangle \sim r^0$ is roughly constant. Plugging this expression into equation 1, we obtain the energy scaling $E(\kappa) \sim \kappa^{-1}$ observed in figure 4. That is, the fibres decorrelate the flow and reduce the magnitude of the scaling exponent β. Spheres on the other hand can only act as barriers to the flow for separations larger than their diameter c, so we see a departure from Kolmogorov's scaling only at the largest length-scales ($\kappa < \kappa_c = 12.6$) in figure 3a.

To view the length-scales at which the particles act on the flow, we show the spectrum of work done on the fluid by the particles F_{fs} in figure 5. This is the fluid-solid coupling contribution to the turbulent kinetic energy-spectrum balance,

$$\partial_t E(\kappa,t) = T(\kappa,t) + V(\kappa,t) + F_{\text{tur}}(\kappa,t) + F_{\text{fs}}(\kappa,t) \qquad (2)$$

Where T, V, and F_{tur} are the rate of work done on the fluid by convection, viscous dissipation, and turbulence forcing respectively. We see that the work done by the spheres peaks around $\kappa = 10 \approx \kappa_c$, and makes minimal contribution to the flow at smaller scales ($\kappa > 60$). On the other hand, the work done by the fibres peaks around $\kappa = 100$, and shows a much broader spread in Fourier space. I.e., the spheres act on the fluid at length-scales comparable with their diameter, and the anisotropic particles act at length scales comparable with their thickness d. This is in keeping with the observations of decorrelation made above.

CONCLUSIONS

We have investigated finite sized particle-laden turbulent flows at exceptionally high Reynolds numbers. By contrasting flows with spheres and fibres, we found that particle geometry has profound effects on the mechanisms of turbulence modulation. Even for fibres and spheres of the same size, geometrical effects mean fibres disrupt the entire turbulent energy cascade, whereas spheres do not. However both particle geometries have similar drag enhancing effect on the flow (figure 2). We can assume that particles of intermediate aspect ratios (such as ellipsoids) would have an effect which is qualitatively in between the two cases discussed in this paper, I.e., a micro-scale Reynolds number that decreases with particle mass fraction,

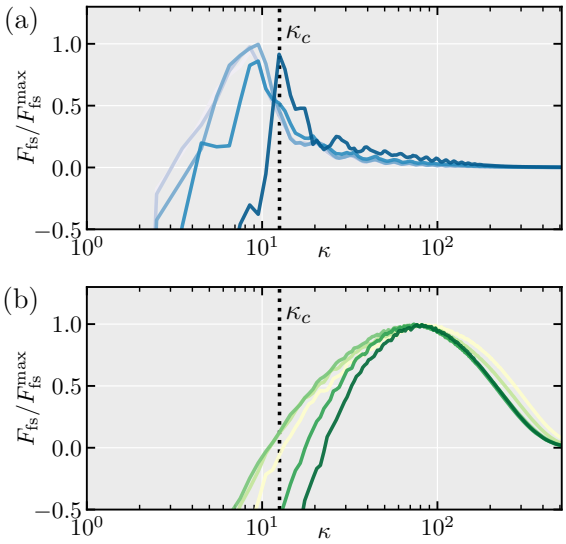

Figure 5. Spectra of the work done on the fluid by the particles F_{fs}, normalised by their peak values $F_{\text{fs}}^{\max}$ for ease of comparison. The work done by spheres is plotted in blue (a), and the work done by fibres is plotted in green (b). The particle mass fraction M for each case is denoted by the brightness of the line colour, using the same colours as the markers in figures 2 and 4. The vertical dotted lines show the wave-number κ_c corresponding to the sphere diameter and fibre length.

and a disruption of Kolmogorov's turbulent cascade at large to intermediate scales. These results have applications in turbulent flow control, E.g., they show that fibres can be added to a fluid in order to reduce velocity correlations and enhance mixing at small scales.

REFERENCES

Andersson, H. I., Zhao, L. & Barri, M. 2012 Torque-coupling and particle–turbulence interactions. *J. Fluid Mech.* **696**, 319–329.

Ardekani, M. N., Rosti, M. E. & Brandt, L. 2019 Turbulent flow of finite-size spherical particles in channels with viscous hyper-elastic walls. *J. Fluid Mech.* **873**, 410–440.

Balachandar, S. & Eaton, J. K. 2010 Turbulent dispersed multiphase flow. *Annu. Rev. Fluid Mech.* **42**, 111–133.

Brandt, L. & Coletti, F. 2021 Particle-laden turbulence: Progress and perspectives. *Annu. Rev. Fluid Mech.* **54**, 159–189.

Breard, E. C. P., Lube, G., Jones, J. R., Dufek, J., Cronin, S. J., Valentine, G. A. & Moebis, A. 2016 Coupling of turbulent and non-turbulent flow regimes within pyroclastic density currents. *Nat. Geosci.* **9** (10), 767–771.

Cannon, I., Izbassarov, D., Tammisola, O., Brandt, L. & Rosti, M. E. 2021 The effect of droplet coalescence on drag in turbulent channel flows. *Phys. Fluids* **33** (8), 085112.

Capecelatro, J., Desjardins, O. & Fox, R. O. 2018 On the transition between turbulence regimes in particle-laden channel flows. *J. Fluid Mech.* **845**, 499–519.

De Lillo, F., Cencini, M., Durham, W. M., Barry, M., Stocker, R., Climent, E. & Boffetta, G. 2014 Turbulent fluid acceleration generates clusters of gyrotactic microorganisms. *Phys. Rev. Lett.* **112** (4), 044502.

Dodd, M. S. & Ferrante, A. 2016 On the interaction of Taylor

length scale size droplets and isotropic turbulence. *J. Fluid Mech.* **806**, 356–412.

Elghobashi, S. 1994 On predicting particle-laden turbulent flows. *Appl. Sci. Res.* **52** (4), 309–329.

Falkinhoff, F., Obligado, M., Bourgoin, M. & Mininni, P. D. 2020 Preferential concentration of free-falling heavy particles in turbulence. *Phys. Rev. Lett.* **125** (6), 064504.

Freund, A. & Ferrante, A. 2019 Wavelet-spectral analysis of droplet-laden isotropic turbulence. *J. Fluid Mech.* **875**, 914–928.

Gualtieri, P., Picano, F., Sardina, G. & Casciola, C. M. 2013 Clustering and turbulence modulation in particle-laden shear flows. *J. Fluid Mech.* **715**, 134–162.

Hori, N., Rosti, M. E. & Takagi, S. 2022 An eulerian-based immersed boundary method for particle suspensions with implicit lubrication model. *Comput. Fluids* p. 105278.

Huang, W.-X., Shin, S. J. & Sung, H. J. 2007 Simulation of flexible filaments in a uniform flow by the immersed boundary method. *J. Comput. Phys.* **226** (2), 2206 – 2228.

Kane, Ian A. & Clare, Michael A. 2019 Dispersion, Accumulation, and the Ultimate Fate of Microplastics in Deep-Marine Environments: A Review and Future Directions. *Frontiers in Earth Science* **7**, 80.

Kim, Yongsam & Peskin, Charles S 2007 Penalty immersed boundary method for an elastic boundary with mass. *Phys. Fluids* **19** (5), 053103.

Lucci, F., Ferrante, A. & Elghobashi, S. 2010 Modulation of isotropic turbulence by particles of Taylor length-scale size. *J. Fluid Mech.* **650**, 5–55.

Lundell, Fredrik, Söderberg, L. Daniel & Alfredsson, P. Henrik 2011 Fluid Mechanics of Papermaking. *Annual Review of Fluid Mechanics* **43** (1), 195–217.

Maxey, M. 2017 Simulation methods for particulate flows and concentrated suspensions. *Annu. Rev. Fluid Mech.* **49**, 171–193.

Olivieri, Stefano, Akoush, Assad, Brandt, Luca, Rosti, Marco E & Mazzino, Andrea 2020*a* Turbulence in a network of rigid fibers. *Phys. Rev. Fluids* **5** (7), 074502.

Olivieri, Stefano, Brandt, Luca, Rosti, Marco E & Mazzino, Andrea 2020*b* Dispersed fibers change the classical energy budget of turbulence via nonlocal transfer. *Phys. Rev. Lett.* **125** (11), 114501.

Olivieri, S., Mazzino, A. & Rosti, M. E. 2021 Universal flapping states of elastic fibers in modulated turbulence. *Phys. Fluids* **33** (7), 071704.

Podvigina, O. & Pouquet, A. 1994 On the non-linear stability of the 1: 1: 1 abc flow. *Phys. D: Nonlinear Phenomen.* **75** (4), 471–508.

Pope, S. B. 2000 *Turbulent Flows*. Cambridge University Press.

Rosti, Marco Edoardo & Brandt, Luca 2020 Increase of turbulent drag by polymers in particle suspensions. *Phys. Rev. Fluids* **5** (4), 041301.

Rosti, M E, Cavaiola, M, Olivieri, S, Seminara, A & Mazzino, A 2021 Turbulence role in the fate of virus-containing droplets in violent expiratory events. *Phys. Rev. Research* **3** (1), 013091.

Rosti, M. E., Ge, Z., Jain, S. S., Dodd, M. S. & Brandt, L. 2019 Droplets in homogeneous shear turbulence. *J. Fluid Mech.* **876**, 962–984.

Rosti, M. E., Olivieri, S., Banaei, A. A., Brandt, L. & Mazzino, A. 2020*a* Flowing fibers as a proxy of turbulence statistics. *Meccanica* **55**, 357 – 370.

Rosti, M. E., Olivieri, S., Cavaiola, M., Seminara, A. & Mazzino, A. 2020*b* Fluid dynamics of covid-19 airborne infection suggests urgent data for a scientific design of social distancing. *Sci. Rep.* **10** (1), 1–9.

Sengupta, A., Carrara, F. & Stocker, R. 2017 Phytoplankton can actively diversify their migration strategy in response to turbulent cues. *Nature* **543** (7646), 555–558.

Sozza, A., Cencini, M., Musacchio, S. & Boffetta, G. 2020 Drag enhancement in a dusty Kolmogorov flow. *Phys. Rev. Fluids* **5** (9), 094302.